Chapter 9

Function Scaling and Adaptive Boundary Condition Throttling for Convergence Control in Highly Nonlinear Poisson–Boltzmann Electrolyte Models

Drew F. Parsons, Matteo Farci, Alin Grigoras, and Dagmawi Tadesse

Abstract The Poisson–Boltzmann (PB) model of electrolyte solutions combines the Poisson equation for electrostatic potentials with a Boltzmann equation $c = c_0 \exp[-e\psi/kT]$ for mobile ion concentrations that is highly nonlinear once the electrostatic potential exceeds 0.1 V. This introduces numerical challenges: first, suitable convergence conditions for the concentration functions become sensitive to the boundary potential. Second, a controlled initial guess must be provided to avoid the finite element method calculation diverging to NaN. We resolve the first challenge by logarithmically scaling the concentration function. A nontrivial log-zero scaling function can handle the near-zero concentrations of coions in a classical point charge model, though is redundant in an advanced model that includes steric forces due to finite ion sizes. The second challenge is resolved with an adaptive throttling algorithm that throttles large values of boundary conditions down to the level of the linear regime and then iteratively raises the throttle until the final nonlinear solution is obtained. The combination of a steric model and throttling enables computation of concentrated electrolytes with electrode potentials as high as 2,000 V. We provide a general derivation of the weak and strong forms of the PB system from the underlying thermodynamic energy functional.

D. F. Parsons e-mail: drew.parsons@unica.it
Department of Chemical and Geological Sciences, University of Cagliari, Cagliari, Italy,

M. Farci
Department of Chemical and Geological Sciences, University of Cagliari, Cagliari, Italy,

A. Grigoras
Department of Chemical and Geological Sciences, University of Cagliari, Cagliari, Italy,

Dagmawi Tadesse
School of Mathematics, Statistics, Chemistry and Physics, Murdoch University, Murdoch, WA, Australia

J. S. Dokken et al. (eds.), *The FEniCS Project*,
Simula SpringerBriefs on Computing 19,
https://doi.org/10.1007/978-3-032-17396-6_9

Introduction

Continuum theory (mean field theory) has been an effective tool for studying the behaviour of systems in electrolyte solutions. The Poisson–Boltzmann (PB) model (Wu, 2022) enables evaluation of ion adsorption layers at surfaces together with the electric field generated by surface charge and adsorbed ions. The PB model underpins the theory of stability of microparticle suspensions in aqueous media, enabling the modelling of particle aggregation and surface forces. The same theory can also be applied to model electrochemical systems, including energy storage devices, batteries, or supercapacitors. However, there is a crucial difference in the two classes of applications that has a significant impact on the numerical stability of the model. The surface potentials of typical microparticles, such as protein molecules or metal oxide particles, tend to lie in the range 5–50 mV, which is 0.2–2 kT in thermal energy units (based on a thermal potential at $T = 298$ K defined by $e\psi_T = kT$, where e is the elementary charge, k is Boltzmann's constant, and T is temperature). Electrolytic energy storage systems, by contrast, typically operate with electrode potentials on the order of 1–5 V, that is, 1,000–5,000 mV, or 40–200 kT. The nonlinearity of the PB model is highly sensitive to energies exceeding one kT unit, requiring particular algorithms to enable numerical nonlinear convergence. Our goal is to set up the calculation to solve successfully over a broad range of electrode potentials without requiring the manual readjustment of convergence parameters. We identify two main steps, implemented via finite element methods using FEniCSx (Baratta et al., 2023): the log scaling of ion concentration functions and the adaptive throttling of boundary conditions.

For context, we first present a summary of the physics and derive the weak and strong formulations defining the PB model from the underlying thermodynamic energy functional. The derivation is general, allowing for spatially varying permittivity, although we employ a dielectric constant in the calculations here. The derivation allows for non-electrostatic interactions of the electrolyte, particularly steric forces due to finite ion size effects. To focus on the numerical algorithms, we omit redox phenomena (including the electrolysis of water) that would occur in real systems at high electrode potentials.

9.1 Weak Formulation of the PB Model

The energy functional for an electrolyte solution determined by electrostatic potential $\psi(x)$ and ion concentration profiles $c_i(x)$ can be composed from various fundamental energy contributions, as follows:

$$\Omega[\psi, c_i] = \Omega_{el} + \Omega_{en} + \Omega_{ex}, \tag{9.1}$$

where Ω_{el} describes the direct energy of the electrostatic field generated by the electric charge of ions and surfaces (Jackson, 1999):

$$\Omega_{el} = \frac{1}{2}\int_V D \cdot E dx = -\frac{1}{2}\int_V D \cdot E dx + \sum_i \int_V z_i e c_i(x)\psi(x)dx + \int_S \sigma(s)\psi(s)ds, \tag{9.2}$$

with E denoting the electric field, $E = -\nabla\psi$; D the electric displacement, $D = \varepsilon_0\varepsilon(x)E$; ε_0 the permittivity of the vacuum; $\varepsilon(x)$ the (spatially varying) relative permittivity; z_i the valency of ion i; and $\sigma(s)$ the surface charge density on boundary S. Here, V refers to the domain (volume) of the system in space.

The term Ω_{en} describes the ideal entropic energy of ions, treated as ideal (non-interacting) particles (Gray and Stiles, 2018; Tadesse and Parsons, 2024):

$$\Omega_{en} = kT\sum_i \int_V \left[c_i(x)\ln\left(\frac{c_i(x)}{c_{i\infty}}\right) - c_i(x) + c_{i\infty}\right] dx, \tag{9.3}$$

where $c_{i\infty}$ is the bulk concentration of ions. As a point of physics, it is important to note that the use of a fixed bulk concentration means the system is controlled by the chemical potential of ions, with a variable number of ions in the domain V of interest. In other words, the thermodynamic potential is a grand potential, not (Helmholtz) free energy, and for that reason we write the energy as Ω rather than F. A free energy formulation (with a fixed number of ions) would require the use of a thermal de Broglie wavelength instead of $c_{i\infty}$ (Gray and Stiles, 2018).

The grand potential term $\Omega_{el} + \Omega_{en}$ defines the conventional PB model. The term Ω_{ex} represents extra contributions to the total energy functional that describe other relevant physics, such as pH-dependent charge regulation (Parsons and Salis, 2019), specific ion interactions (Parsons et al., 2022), or steric forces due to finite ion size (López-García et al., 2018). We consider the latter in this work.

The PB model describes the system in equilibrium, obtained by minimizing the total grand potential with variation $\delta\Omega = 0$ with respect to ψ and c_i. Variation with respect to ψ (with a test function $p \equiv \delta\psi$) leads to a weak formulation for the Poisson equation

$$0 = -\int_V \varepsilon_0\varepsilon(x)(\nabla\psi, \nabla p)dx + \sum_i z_i e\int_V c_i(x)pdx + \int_{S_N}\sigma(s)pds \tag{9.4}$$

for all test functions p in the relevant function space (vanishing on the Dirichlet boundary subdomain $S_D \subset S$). A Dirichlet boundary condition $\psi(x) = \psi_0$ for $x \in S_D$ can be applied to set a defined potential, for instance, the potential of an electrode controlled by a potentiostat. For other boundary subdomains $S_N = S \setminus S_D$, a Neumann boundary condition can be set via the surface charge density σ in the surface term, applying Gauss' law at the external boundary,[1]

[1] At an internal boundary, $\sigma = D_\perp^{\text{out}} - D_\perp^{\text{in}}$.

$$\sigma = -D_{\perp} = (n, \varepsilon_0 \varepsilon \nabla \psi), \tag{9.5}$$

where $D_{\perp}$ is the transverse component of the electric displacement vector D at the boundary, or, equivalently, n is the outward normal vector at the boundary. Here, (9.5) is valid across the entire external surface S but sets a Neumann boundary condition when applied to the surface subdomain S_N in (9.4). Applied at S_D, (9.5) evaluates the surface charge density generated at Dirichlet surfaces. After additional integration by parts, the weak formulation (9.4) leads to the strong formulation of the electrostatic Poisson equation, $\nabla \cdot D = \sum_i z_i e c_i(x)$.

The variation of Ω with respect to each ion concentration profile c_i (in turn, with test functions $b_i \equiv \delta c_i$), assuming linear variations such that $\ln(1 + b_i/c_i) \approx b_i/c_i$, leads to the weak formulation of Boltzmann's equation,

$$0 = \int_V \left[e z_i \psi(x) + kT \ln\left(\frac{c_i(x)}{c_{i\infty}}\right)\right] b_i dx, \tag{9.6}$$

for all test functions b_i. The strong form of the classical Boltzmann equation, $c_i(x) = c_{i\infty} \exp(-z_i e \psi(x)/kT)$, can then be obtained. The Boltzmann equation is implicitly controlled by the bulk concentrations $c_{i\infty}$, and an explicit boundary condition for the concentration functions is not needed.

9.1.1 Non-electrostatic Interactions: A Steric Model with Finite Ion Size

In the classical point charge PB model, the ion concentrations c_i are determined completely by the electrostatic potential with the Boltzmann equation in closed form, such that only the Poisson equation would need to be solved directly. However, the physical problem with the classical model is evident in electrochemical systems with an electrode potential of 1 V. A 1 V potential is equivalent to a thermal energy of $40kT$ (at room temperature), for which the conventional Boltzmann factor for a counterion is $\exp(40) \approx 2.3 \times 10^{17}$. That is, the surface counterion concentration of a 1M electrolyte would exceed 10^{17} mol/L, which is clearly unphysical. We return the model to physical relevance by adding an extra steric energy term Ω_{ex} with corresponding excess chemical potential per ion μ_i^{ex}, for which the modified Boltzmann equation is

$$c_i(x) = c_{i\infty} \exp\left[-(z_i e \psi(x) + \mu_i^{ex}(x) - \mu_{i\infty}^{ex})/kT\right]. \tag{9.7}$$

This corresponds to a total chemical potential $\mu_i(x)$ for each ion, defined by

$$\mu_i(x) = \mu_i^{\text{entropic}} + \mu_i^{\text{electrostatic}} + \mu_i^{ex} \tag{9.8}$$

$$= \mu_{i\infty} + kT \ln(c_i(x)/c_{i\infty}) + e z_i \psi(x) + \mu_i^{ex}(x) - \mu_{i\infty}^{ex}, \tag{9.9}$$

where $\mu_{i\infty}$ refers to the (fixed) excess chemical potential of the ion in bulk solution, defined relative to an ideal unit reference solution by $\mu_{i\infty} = kT \ln c_{i\infty} + \mu_{i\infty}^{ex}$. The steric model we employ is the Carnahan–Starling (CS, 1969) model, with a contribution to the grand potential

$$\Omega_{ex} = \sum_i \int_V c_i(x) \left[kT \frac{4\phi - 3\phi^2}{(1-\phi)^2} - \mu_{i\infty}^{ex} \right] dx \tag{9.10}$$

and the weak formulation

$$0 = \int_V (\mu_i^{ex} - \mu_{i\infty}^{ex}) b_i \, dx \tag{9.11}$$

for all b_i, which is added to (9.6), the weak formulation for the Boltzmann equation, together generating the strong formulation of the modified Boltzmann equation, (9.7). Here the excess chemical potential per ion for the CS model, corresponding to the energy functional (9.10), is

$$\mu_i^{ex} = kT \frac{\phi(8 - 9\phi + 3\phi^2)}{(1-\phi)^3}, \tag{9.12}$$

where ϕ is the *total* ion volume fraction defined by $\phi = \sum_i c_i v_i$, with v_i the intrinsic molar volume per ion i. Hence the CS excess chemical potential is defined identically for all ions.

To derive the weak formulation in (9.11), we applied a homogenized component approximation that assigns common volumes at the point of introducing the variation δc_i (i.e. the test function b_i), such that $\delta\phi = v_j \delta c_i$ rather than $v_i \delta c_i$. This approximation is required since the CS model was formulated for single-component systems. The more complex multicomponent Boublík–Mansoori–Carnahan–Starling–Leland model would enable ion-specific chemical potentials (Mansoori et al., 1971), removing the need for this approximation. The terms ϕ_∞, $\mu_{i\infty}^{ex}$ are the bulk total volume fraction and excess chemical potential defined by bulk concentrations $c_{i\infty}$. With this term, the Boltzmann equation (9.7) becomes transcendental in c_i, precluding a closed expression that would determine ion concentrations. Concentration functions must therefore be explicitly solved numerically alongside the potential ψ. In this paper, we address strategies for managing the strong nonlinearity in the system introduced by this term in the presence of large values of the potential. Note that c_i must also be solved explicitly in the case of time-dependent nonequilibrium Poisson–Nernst–Planck (drift–diffusion) systems (López-García et al., 2018) where ion concentrations are not in equilibrium and are determined by a continuity equation rather than a Boltzmann equation.

We note one last point on the weak formulation of the Boltzmann equation. The variational derivation of these weak formulations from the energy functionals, (9.6) and (9.11), presents them in terms of the chemical potential of the ions, (9.9), and not the concentration directly. That is, fundamentally, the strong form of the Boltzmann

equation is simply $\mu_i(x) = \mu_{i\infty}$, the condition of equal chemical potential at all points in the domain in equilibrium with an external bulk bath. The Boltzmann equation in terms of concentration, (9.7), is then simply a rearrangement of the strong equation for chemical potential. Chemists are in the habit of using the Boltzmann equation in the concentration form rather than the chemical potential. Our implementation in code therefore applies the weak form of the Boltzmann equation via concentrations, as

$$0 = \int_V \left[c_i(x) - c_{i\infty} e^{-(z_i e \psi(x) + \mu_i^{ex}(x) - \mu_{i\infty}^{ex})/kT} \right] b_i dx \tag{9.13}$$

for all test functions b_i, rather than applying it via the chemical potential components in (9.6) and (9.11). Because the concentration functions $c_i(x)$ being solved are the same, this change in the weak form should not affect residuals. These alternative weak forms for the Boltzmann equation may affect efficiency, perhaps by changing the condition number of the matrices involved. Our testing finds the chemical potential formulation to be less stable than the concentration formulation, failing to converge with a 1 V electrode potential, where the latter weak form achieves successful convergence with the log-zero concentration scaling described below.

9.2 Numerical Convergence

9.2.1 Graded Mesh

Solution of the nonlinear PB model requires a finer mesh in the region close to an electrode boundary, rendering solutions on a uniform linear mesh impractical at electrode potentials greater than 0.1 V. The general exponential nature of the potential, $\psi(x) \sim \psi_0 \exp(-\kappa x)$, suggests that logarithmic spacing of the mesh may be suitable. A graded mesh spacing can be achieved with a geometric sequence of mesh points to obtain finer spacing for the points closer to the boundary. For the simple planar geometry of a flat electrode located at $x = 0$, where x is the perpendicular distance from the boundary, we take a uniformly spaced set of $s \in [0, 1]$ (e.g. $s = x'/L$ for an initially uniformly spaced $x' \in [0, L]$) and obtain a sufficiently well-graded mesh with

$$x = s^3 L. \tag{9.14}$$

Symmetry renders the system of the flat electrode essentially one-dimensional along the perpendicular x-coordinate, although the calculation can be performed in a 2D or 3D geometry. Whether in 1D, 2D, or 3D, the same graded mesh can be applied along the x-direction. For more complex non-planar geometries, adaptive mesh refinement would be suitable, likely controlled by the magnitude of the gradient of the electrostatic potential (i.e. the electric field) or by concentration gradients.

The Debye length (electrostatic screening length) of the electrolyte provides a natural reference for the units of L. The Debye length is the decay length of the exponential

decaying profile of the potential $\psi(x)$ found far from the electrode, where its magnitude has fallen below 25 mV. The distance to zero potential (bulk solution) may be taken as $L = 10 - 30$ Debye lengths, depending on one's tolerance for 'zero'. The Debye length itself could be taken as the length unit for L, but typical Debye lengths lie in the nanoscale, ranging from 0.5 nm for seawater (0.5M salt) to 1,000 nm for pure water (due to H^+ and OH^- from dissociated water). We use nanometres as the units for L to facilitate the comparison of length scales in different systems, setting L at approximately 30 Debye lengths (in nanometres) to reach bulk solution. At higher potentials, above 100 V, we amplify that value of L by a factor of two to allow for the formation of a steric counterion adsorption layer before the decay region is reached (Tadesse and Parsons, 2022).

9.2.2 Solver Description

We constructed a finite element implementation of the weak formulation ((9.4) and (9.13)) in FEniCSx (Baratta et al., 2023), using continuous Lagrange elements of polynomial order 2 (linear elements with order 1 can also be used). The electrolyte solution is taken as NaCl with bulk concentration 1 mol/L. To illustrate general issues of nonlinear convergence, we calculate the electrostatic and ion concentration profiles of ions adsorbed at a single flat electrode surface along the direction perpendicular to the surface, with the electrode boundary at $x = 0$. The electrode potential is controlled (Dirichlet boundary condition), and the bulk solution is represented by a zero Neumann condition (zero net charge, zero electric field) at a distance of 10 nm (30 Debye lengths for the 1M electrolyte). Nonlinear solutions are computed using FEniCSx's `NonlinearProblem` with a standard Newton solver. The convergence criterion is set to DOLFINx's default 'incremental' method with absolute tolerance 10^{-5}. We set PETSc options (Balay et al., 2023; Dalcin et al., 2011) configuring the solver to use the LU direct solver provided by MUMPS (Amestoy et al., 2001, 2019), with the PETSc Krylov type set to apply the preconditioner only once (`ksp_type="preonly"`, `pc_type="lu"`, `pc_factor_mat_solver_type="mumps"`). By contrast, for instance, a conjugate gradient solver (`ksp_type="cg"`, `pc_type="gamg"`) generates a spurious oscillatory electrostatic potential profile with electrode potentials higher than 0.1 V.

In our implementation, we have adopted nanometres for the length scale of the mesh (x). The physical units for real electrostatic potentials $\psi(x)$ and concentration functions $c_i(x)$, are volts and M (mol/L), respectively. However, in computations we used units for the potential and concentration functions scaled to unity, as described next.

9.2.3 Function Scaling

The electrostatic potential $\psi(x)$ is handled with trivial scaling, solving $P(x) = \psi(x)/\psi_0$, where ψ_0 is the electrode potential. However, we must take more care scaling the concentration functions $c_i(x)$. We already noted that the counterion concentration becomes unphysically large in the conventional point charge model due to nonlinear exponentiation of electrostatic potentials exceeding 0.1–0.2 V in the Boltzmann equation. Trivial scaling can be introduced by solving the concentration function scaled against the bulk concentration, but the nonlinear catastrophe is reached numerically above 0.5 V. At 0.6 V, the conventional calculation with simple scaling is already unable to reduce the residual below the required convergence criterion 10^{-5}. While it would be possible to relax the convergence tolerance to obtain a reasonable solution, our aim is to obtain a robust general solver that does not require the close manipulation of convergence criteria. For instance, modelling the cyclic voltammetry curve of an electrode may require calculations over a potential window as wide as −5 V to 5 V.

The challenge arises due to the extreme magnitudes of the counterion concentration at the electrode surface. The weak formulation for the Boltzmann equation in (9.6) suggests a solution: solve for the concentration function in log form,

$$C_i(x) = \ln[c_i(x)/c_{i\infty}], \tag{9.15}$$

rather than the physical concentration function $c_i(x)$ directly. Log scaling extends the solvability of the conventional point charge PB model up to electrode potentials as high as 1.5 V. Solutions for the electrostatic potential and counterion concentration profile are presented in Fig. 9.1. Shown on a log scale, strong nonlinearity in the PB system becomes apparent in the bend in the electrostatic potential (Fig. 9.1a) close to the surface ($x < 2$Å) for electrode potentials > 0.2 V.

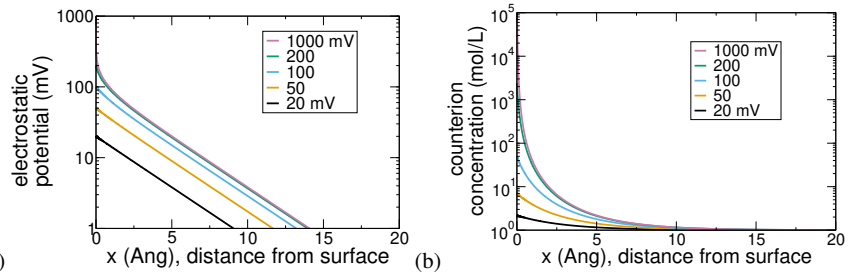

Fig. 9.1: Solutions to the classical point charge PB model of a 1M NaCl electrolyte solution, shown as profiles along x, the perpendicular distance from an electrode surface. (a) Electrostatic potential. (b) Counterion (Cl^-) concentration.

At still higher potentials, the stability of simple log scaling with respect to the coion must be considered. The coion, with the same charge as the electrostatic potential, is repelled from the electrode surface, resulting in coion concentrations trending towards zero near the electrode. At sufficiently high potentials, this generates values in the log-scaled function that tend towards $-\infty$, which destabilizes the numerical solution (residuals become infinite). We therefore introduce a more complex log-scaling function,

$$Z_i(x) = \ln\left[c_i(x)/c_{i\infty} + 1\right]/\ln 2 - 1, \tag{9.16}$$

which keeps the scaled coion function constrained between -1 and zero rather than between $-\infty$ and zero. Since this scaling function addresses the near-zero concentration of the coion, we call it log-zero scaling.

9.2.4 Throttling Algorithm

The log-zero scaling of concentration functions facilitates a successful numerical solution to the conventional PB equation at electrode potentials exceeding 1 V. Nevertheless, Fig. 9.1(b) demonstrates the point charge catastrophe of the conventional model with counterion concentrations exceeding 10^5 mol/L at the electrode surface. Moreover, for general electrochemical applications, solutions for electrode potentials higher than 1.5V are required. To address the physical problem, we introduce finite ion sizes with a steric force provided by the Carnahan–Starling model, (9.12) (with weak form (9.11)). We apply ion volumes $v_{Na} = 1.24\text{Å}^3$ per Na^+ ion and $v_{Cl} = 35.9\text{Å}^3$ per Cl^- ion (these are the quantum mechanical volumes of the electron clouds (Parsons and Ninham, 2009)).

The additional nonlinearity introduced by the Carnahan–Starling model, where the chemical potential depends on the concentrations being calculated, introduces a new challenge. The default nonlinear solver in FEniCSx assumes zero as an initial guess for the functions being solved. However, under the nonlinear conditions (with electrode potential > 0.2 V) where the Carnahan–Starling steric force is required, the zero initial guess quickly leads to a diverging solution with an infinite or NaN residual. A stable solution, however, is accessible at lower values of the boundary condition. We nudge the solver to a stable solution by applying a throttling algorithm: reduce the boundary condition to a small value for which a solution can be obtained and then incrementally increase the boundary value back towards the target value, using the previously found solution as an initial guess for the next iteration. This approach is known to mathematicians as a homotopy method (Liao, 2012) or numerical continuation method (Allgower and Georg, 1990), with our throttle serving as a homotopy parameter applied to boundary conditions. A flowchart for the algorithm is shown in Fig. 9.2.

The throttle is a multiplier applied to the magnitude of the boundary conditions. If the solver fails to converge, then we reduce the throttle downwards by bisection between

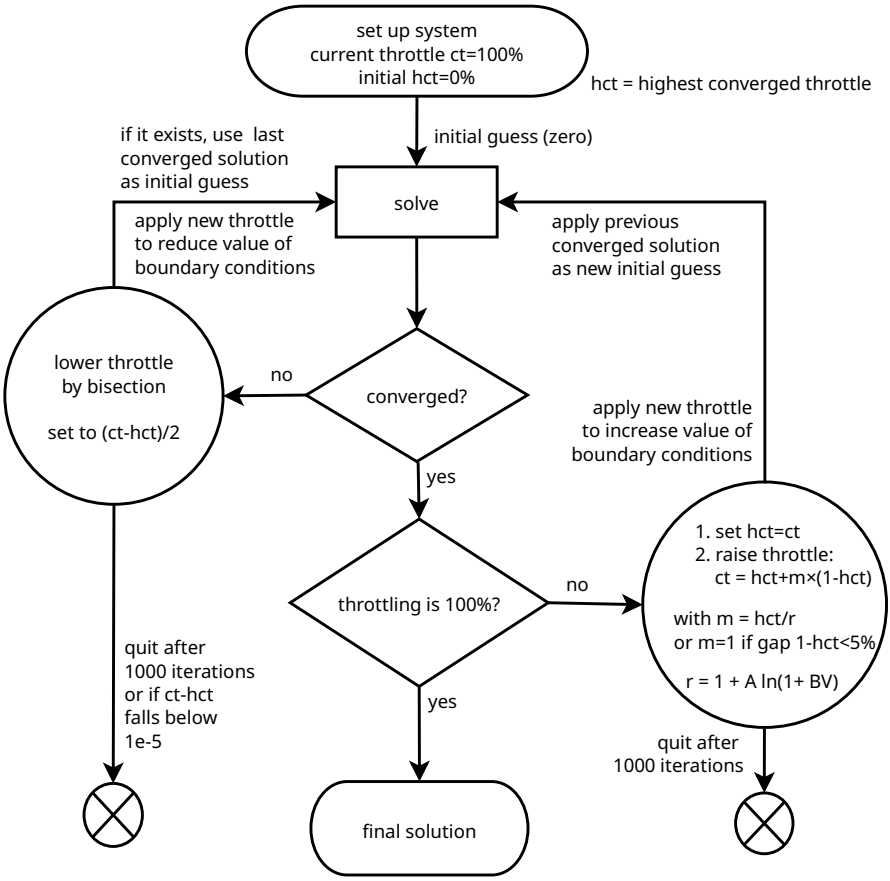

Fig. 9.2: Flowchart for the throttling algorithm

the current failed value (current throttle, ct) and the highest converged throttle (hct, initially zero). Once the boundary condition is throttled low enough to generate a converged solution, we update the hct and raise the throttle upwards by an amount u, closing the gap towards 100% (we set the throttle to 100% if the procedure would exceed it). The value of u must find a balance between reaching a 100% throttle in as few iterations as possible (do not make u too small), while not collapsing back to non-converging conditions when raising the throttle (do not make u too large). Empirically, we find that, when the hct is small, the rise rate must also be small to obtain the next converged iteration. Once the hct is large, the rise rate may be proportionally larger. We therefore propose a rise step $u = m \times (1 - \text{hct})$ such that the next throttle applied after a converged iteration is

$$\text{ct}[\text{new}] = \text{hct} + m(1 - \text{hct}), \tag{9.17}$$

with

$$m = \begin{cases} \dfrac{\text{hct}}{r} & , \\ 1 & \text{if } 1 - \text{hct} < 5\%. \end{cases} \tag{9.18}$$

This produces a quadratically accelerating rise rate and attempts a direct jump to 100% once the remaining gap is less than 5%. It is likely that our formulation, quadratic in the hct term, approximates a more optimal exponential (or sigmoidal) rise rate.

Optimal Throttling. An example of the throttle rate against the number of iterations is presented in Fig. 9.3 for 1 V and 10 V boundaries with different choices of fixed values of the rise rate multiplier r. A best value of r can be identified for each voltage, minimizing the number of iterations required, for example, $r = 2$ for 1 V and $r = 3$ for 10 V. A value of r larger than the best value means the rise step is smaller, such that convergence is smooth, but requires more iterations. A lower value of r means the rise step is too large, overstepping and resulting in a nonconverging iteration, such that more iterations are required to fall back to a converging throttle rate.

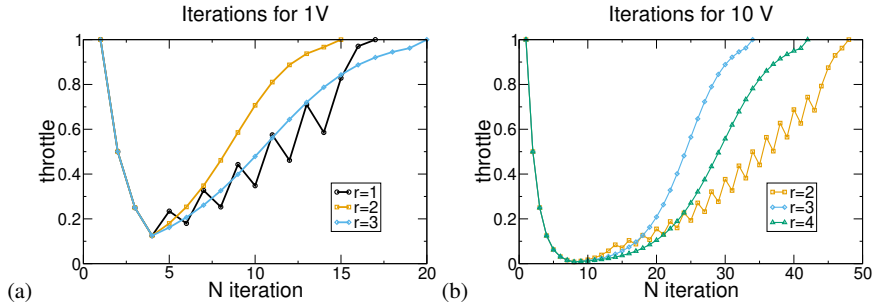

Fig. 9.3: Attempted throttle rate versus iteration numbers for (a) 1 V and (b) 10 V boundaries with fixed rise rate multipliers $r = 1, 2, 3$, and 4. The steric model is solved with log-zero scaling.

The best-performing fixed values of r for potentials up to 100 V are presented in Fig. 9.4. We observe a similar trend in 1D calculations with trivial and log-zero function scaling (the differences may not be significant, since only integer values of r up to 10 were tested). A priori, we have no reason to expect the optimal value of r to be universal, and we might expect it to vary with conditions such as the electrolyte concentration or dimensionality. However, we plot the best r values for trivial scaling over a wide range of concentrations (1D calculations), as well as 2D and 3D calculations of the flat electrode (at a 1M concentration). In all cases, the best $r(V)$ essentially follows the same curve, with a small deviation seen only at 1–2 V, which can be attributed simply to the integer resolution of the simulation. The time per iteration varies with system conditions and dimensionality, but the optimal $r(V)$

for minimizing the number of iterations remains the same. The optimal $r(V)$ can be considered to be universal.

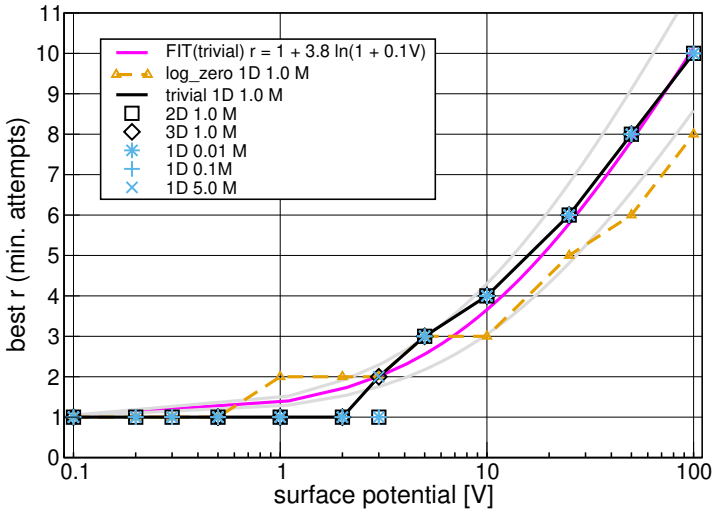

Fig. 9.4: Best fixed rate multiplier r for each voltage, with the lowest number of throttling iterations. The steric model is solved with both trivial (in black) and log-zero (orange dashed line) concentration scaling (1D calculation at a 1M electrolyte concentration). We also show the best r values for 1D calculations with trivial scaling over a range of concentrations (blue stars) and 2D and 3D calculations (black boxes) of a flat electrode at a 1M concentration. The solid purple line denotes the model $r(V) = 1 + 3.78\ln(1 + 0.102V)$ fitted to trivial scaling data. The grey lines mark uncertainty bounds of one standard deviation in the fitted parameters.

Adaptive Throttle Rate. The trend in the best-performing r values shown in Fig. 9.4 suggests that an optimal multiplier follows $r \propto \ln V$, indicating that r may be tuned adaptively to provide the maximum possible rise rate (smallest possible r) that minimizes the number of unsuccessful non-converged attempts for the given boundary condition. A milder rise rate (larger r) is required at larger surface potentials. Allowing for a finite value of r when $V \to 0$, we propose an adaptive definition of r,

$$r(V) = 1 + A\ln(1 + BV). \tag{9.19}$$

This model imposes the limit $r \to 1$ as $V \to 0$. In principle, an optimal low-voltage multiplier might allow $r < 1$ if $r >$hct, but the limit of one is simpler, avoiding the need to compare against the hct. Fitting against the best r values for trivial scaling results in $A = 3.78 \pm 0.36$ and $B = 0.102 \pm 0.020\ \mathrm{V}^{-1}$. The uncertainties here have been determined from the covariance matrix generated by the fitting procedure implemented in the `curve_fit` function provided by the `optimize` module in SciPy (Vugrin et al., 2007). The best r value for log-zero scaling is similar. One could

separately fit parameters for log-zero scaling (to obtain $A = 1.3 \pm 0.2$ and $B = 0.7 \pm 0.5\ \mathrm{V}^{-1}$). Nevertheless, Fig. 9.4 shows that the log-zero data points lie only one standard deviation below the trivial scaling fit. Statistically, there is no significant difference in the best r values for trivial and log-zero scaling.

We emphasize that the value of V used in the adaptive r formula, (9.19), must be the target boundary condition (the final electrode voltage), and not the throttled boundary condition at the given iteration. If a throttled V were applied, r would be small when the boundary condition is strongly throttled, resulting in large rise steps that lead to convergence failure when the target voltage is large.

Table 9.1 shows the number of iterations required to converge with various boundary conditions for the different concentration scaling functions in both the point charge model and the steric model and applying an adaptive $r(V) = 1 + 3.78\ln(1 + 0.102V)$ for 1D meshes with 30 cells. For the point charge model, trivial scaling permits calculations only up to 0.7 V. Log scaling permits calculations up to 0.8 V, and log-zero scaling permits calculations up to 1 V (1.5 V can be reached with a finer mesh).

Pot. (V)	Point Charge			Steric		
	Trivial	Log	Log-Zero	Trivial	Log	Log-Zero
0.1	1	1	1	1	1	1
0.5	1	1	1	1	11	9
0.7	6	1	1	1	11	11
0.8	S	10	6	6	11	11
0.9		S	8	1	14	12
1			7	1	14	12
1.1			F	7	14	14
1.5				10	15	15
2				8	19	16
5				18	27	27
10				27	F	39
100				91		114
1000				439		369
2000				S		762

Table 9.1: Number of throttling iterations required to solve the PB model of a 1M NaCl electrolyte solution for various electrode potentials and concentration scaling functions (trivial, log, or log-zero scaling) for both the classic point charge model and the steric (Carnahan–Starling) model with finite ion sizes. The adaptive rise rate multiplier $r(V) = 1 + 3.78\ln(1 + 0.102V)$ for a 1D mesh with 30 cells. F = failed (throttle step $< 10^{-5}$), and S = stopped at 1,000 iterations.

Trivial scaling is successful for the steric model up to 1,000 V, while simple log scaling fails at 10 V due to instability introduced by near-zero coion concentrations. Log-zero scaling enables calculations to 2,000 V and higher, beyond the limit of trivial scaling. The corresponding performance plot of iterations versus voltage for the steric model (with both trivial and log-zero scaling) is presented in Fig. 9.5. The steric model naturally keeps concentrations within physically reasonable bounds,

such that log-zero scaling is not required for normal electrochemical conditions. Trivial scaling performs better than log-zero scaling when $V < 100$ V, the region of electrochemical interest. Performance is robust with respect to the A and B parameters used to determined $r(V)$, whether fitted to the best r for trivial or log-zero scaling. 2D and 3D calculations generally require the same number of iterations as 1D calculations, showing small differences only at 1–2 V. Even with log-zero scaling, computation of the interaction of 100 kV electrical transmission cables with saline water would require such a large number of iterations that this algorithm would become impractical.

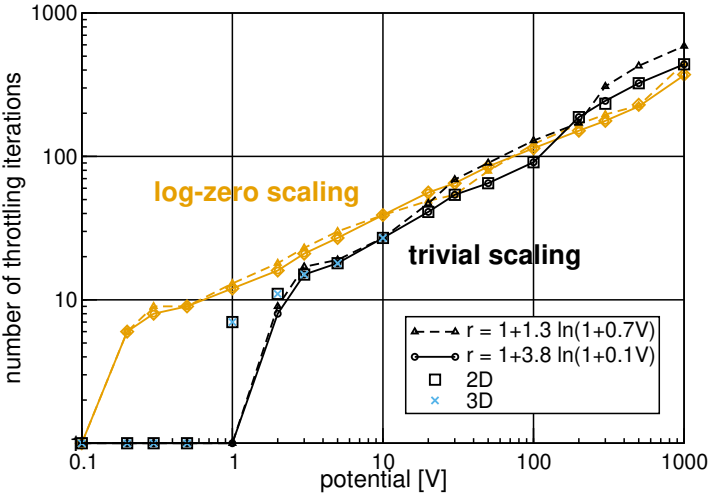

Fig. 9.5: Number of throttling iterations, as a function of electrode voltage, needed to solve the steric model with trivial and log-zero scaling. An adaptive rise rate multiplier $r(V) = 1 + 3.78\ln(1 + 0.102V)$ is used to best fit trivial scaling (solid lines). 1D calculations with trivial scaling are shown in black, and log-zero scaling in orange. The rise rate $r(V) = 1 + 1.3\ln(1 + 0.7V)$ (fitted for the best log-zero value) is also shown (dashed lines) for comparison. 2D data points are indicated by squares (trivial scaling) and diamonds (log-zero scaling). 3D data points (trivial scaling) are denoted by blue crosses.

The sample results of the adaptive throttling algorithm for an electrode charged to 10 V with Carnahan–Starling steric forces are presented in Fig. 9.6, calculated with trivial scaling of the concentration functions with adaptive r coefficients $A = 3.78$ and $B = 0.102\ \mathrm{V}^{-1}$. Figure 9.6(b) shows the onset of a steric adsorption layer (Tadesse and Parsons, 2022) with counterion concentrations constrained below a concentration cap determined by the ion size, a cap of 46 mol/L in the case of our Cl^- ion.

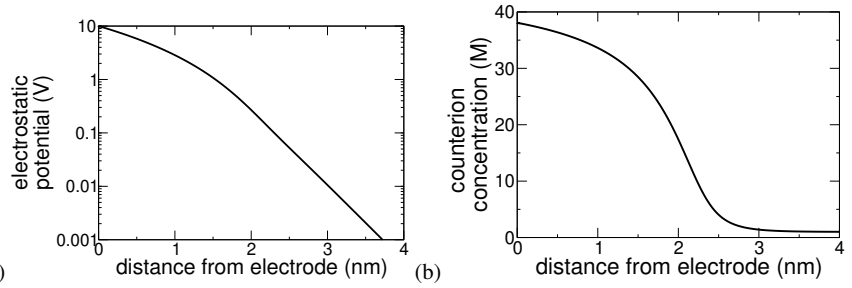

Fig. 9.6: Solutions to the modified PB model of a 1M NaCl electrolyte solution with Carnahan–Starling steric forces, shown as profiles along x, the perpendicular distance from a 10 V electrode surface. (a) Electrostatic potential. (b) Counterion (Cl^-) concentration.

9.3 Conclusion

Modelling complex electrolyte solutions in electrochemical conditions with electrode potentials of 1 V or greater requires both nontrivial physics and nontrivial numerical algorithms. With respect to the physics, aside from redox chemistry and electrolysis (not considered here), the finite sizes of ions must be considered via steric forces. These are expressed as a steric contribution to the chemical potential of ions and used in the underlying thermodynamic energy functional that provides the origin of the weak and strong formulations of the system. To achieve numerical convergence, we propose two steps. First, we propose log-zero function scaling of concentration functions that accounts not only for the heightened concentrations of counterions near an electrode, but also the near-zero concentrations of coions. Second and more importantly, we propose an adaptive throttling algorithm (a kind of homotopy method) that reduces boundary conditions down to the linear regime, where a solution is easily obtained, and then progressively propagates that solution by releasing the throttle until the target boundary condition is obtained. Optimized convergence is obtained by adaptively controlling the rise rate of the throttle factor depending on the target boundary condition.

The combination of log-zero scaling and throttling facilitates calculations of point charge models up to 2 V. Log-zero scaling enables the steric model to reach electrode potentials greater than 2,000 V. However, for typical electrochemical applications with potentials lower than 20 V, where steric forces are needed to maintain the physical relevance of the model, trivial scaling is sufficient and faster than log-zero scaling. The empirical parameters for optimal throttling, minimizing the number of required iterations, appear to be universal, independent of the electrolyte concentration or whether the geometry is 1D, 2D, or 3D. This might indicate a deeper structure in the algorithm that could be revealed with further mathematical analysis. Our 1D, 2D, and 3D simulations tested the same flat electrode surface. We expect the op-

timal throttling conditions will continue to be valid with more complex 3D or 2D geometries, though it may be prudent to confirm this assumption.

We illustrated the throttling algorithm using Dirichlet boundary conditions (electrode potentials), but the principle applies equally to Neumann and more complex boundary conditions.

Acknowledgements We acknowledge the support of a CINECA award under the ISCRA initiative, for the availability of high-performance computing resources and support.

A Python script demonstrating the throttle algorithm is available on Zenodo at `https://doi.org/10.5281/zenodo.14829963`.

References

Allgower EL, Georg K (1990) Numerical Continuation Methods: An Introduction, Springer Series in Computational Mathematics, vol 13. Springer, doi:10.1007/978-3-642-61257-2

Amestoy PR, Duff IS, L'Excellent JY, Koster J (2001) A fully asynchronous multifrontal solver using distributed dynamic scheduling. SIAM Journal on Matrix Analysis and Applications 23:15–41, doi:10.1137/S0895479899358194

Amestoy PR, Buttari A, L'Excellent JY, Mary T (2019) Performance and scalability of the block low-rank multifrontal factorization on multicore architectures. ACM Transactions on Mathematical Software 45:1–26, doi:10.1145/3242094

Balay S, Abhyankar S, Adams M, Benson S, Brown J, Brune P, Buschelman K, Constantinescu E, Dalcin L, Dener A, Eijkhout V, Faibussowitsch J, Gropp W, Hapla V, Isaac T, Jolivet P, Karpeev D, Kaushik D, Knepley M, Kong F, Kruger S, May D, McInnes L, Mills R, Mitchell L, Munson T, Roman J, Rupp K, Sanan P, Sarich J, Smith B, Zampini S, Zhang H, Zhang J (2023) PETSc/TAO Users Manual (Rev. 3.20). doi:10.2172/2205494

Baratta IA, Dean JP, Dokken JS, Habera M, Hale JS, Richardson CN, Rognes ME, Scroggs MW, Sime N, Wells GN (2023) DOLFINx: The next generation FEniCS problem solving environment. doi:10.5281/zenodo.10447666

Carnahan NF, Starling KE (1969) Equation of state for nonattracting rigid spheres. The Journal of Chemical Physics 51:635–636, doi:10.1063/1.1672048

Dalcin LD, Paz RR, Kler PA, Cosimo A (2011) Parallel distributed computing using Python. Advances in Water Resources 34:1124–1139, doi:10.1016/j.advwatres.2011.04.013

Gray CG, Stiles PJ (2018) Nonlinear electrostatics: the Poisson-Boltzmann equation. European Journal of Physics 39:053002, doi:10.1088/1361-6404/aaca5a

Jackson JD (1999) Classical Electrodynamics, 3rd edn. John Wiley & Sons, Inc.

Liao S (2012) Homotopy Analysis Method in Nonlinear Differential Equations, vol 9783642251320. Springer Berlin Heidelberg, doi:10.1007/978-3-642-25132-0

López-García JJ, Horno J, Grosse C (2018) Numerical solution of the electrokinetic equations for multi-ionic electrolytes including different ionic size related effects. Micromachines 9:647, doi:10.3390/mi9120647

Mansoori GA, Carnahan NF, Starling KE, Leland TW (1971) Equilibrium thermodynamic properties of the mixture of hard spheres. The Journal of Chemical Physics 54:1523–1525, doi:10.1063/1.1675048

Parsons DF, Ninham BW (2009) Ab initio molar volumes and gaussian radii. Journal of Physical Chemistry A 113:1141–1150, doi:10.1021/jp802984b

Parsons DF, Salis A (2019) A thermodynamic correction to the theory of competitive chemisorption of ions at surface sites with nonelectrostatic physisorption. Journal of Chemical Physics 151:024701, doi:10.1063/1.5096237

Parsons DF, Carucci C, Salis A (2022) Buffer-specific effects arise from ionic dispersion forces. Physical Chemistry Chemical Physics 24:6544–6551, doi:10.1039/D2CP00223J

Tadesse D, Parsons DF (2024) Thermodynamics beyond dilute solution theory: Steric effects and electrowetting, vol 1-3, Elsevier, pp 126–135. doi:10.1016/B978-0-323-85669-0.00137-9

Tadesse DB, Parsons DF (2022) The impact of steric repulsion on the total free energy of electric double layer capacitors. Colloids and Surfaces A: Physicochemical and Engineering Aspects 648:129134, doi:10.1016/j.colsurfa.2022.129134

Vugrin KW, Swiler LP, Roberts RM, Stucky-Mack NJ, Sullivan SP (2007) Confidence region estimation techniques for nonlinear regression in groundwater flow: Three case studies. Water Resources Research 43:3423, doi:10.1029/2005WR004804

Wu J (2022) Understanding the electric double-layer structure, capacitance, and charging dynamics. Chemical Reviews 122:10821–10859, doi:10.1021/acs.chemrev.2c00097